# Towards integrating 3D printing and automated assembly

Francisco Munguia-Galeano[1], Lesli Ortega-Arroyo[2], Miguel Gabriel Villarreal-Cervantes[3] and Ze Ji[1]

***Abstract*— Recent interest in additive manufacturing (AM) technologies (also known as 3D printing) has led to embedding multi-material and electronic components into 3D-printed structures. However, current 3D printing technologies fail to provide all the required materials to fabricate complex devices. Besides, the process of inserting individual building blocks into the impression is usually carried out manually. This paper presents the design of a robot that integrates 3D printing and automated assembly. The robot utilises two modules. The first module fabricates the body of a device by using fused deposition modelling (FDM) technology. The second module grasps pre-assembled building blocks and inserts them into the device. To this end, the feasibility of this integration is validated with the fabrication of a device (non-fabricable with traditional 3D printers) that contains a development board.**

## I. Introduction

Additive manufacturing (AM), also known as 3D printing, has shown functional capabilities to create geometries which are otherwise difficult or even impossible via classical manufacturing methods (e.g., machining, bulk-forming or sheet-forming) [1]. From early technologies [2] to more recent 3D printing methods, such as fused deposition modelling (FDM) [3], AM technologies have shown a potential to be adopted not only in the manufacturing but also in the construction sector [4].

In the literature, various types of AM processes exist, such as liquid-based, solid-based, and powder-based methods [5]. Liquid-based processes include Fused Deposition Modelling (FDM) [6], Stereolithography (SLA) [7], and PolyJet [8] technologies. Laminated Object Manufacturing (LOM) [9] is an example of a solid-based process. Powder-based processes include Selective Laser Sintering (SLS) [10] and Electron Beam Melting (EBM) [11]. Despite variations in materials and approaches for solidifying them, all of the above technologies share the same fundamental principle of depositing material layer by layer. However, AM technologies are still limited to the main material available for printing. Regarding more complex parts, AM technologies depend on external processes to complete the production process.

Several approaches to overcome this problem have been proposed. For example, Kim et al. [12] introduces a process to insert metallic connections between the layers of 3D-printed structures. In [13], a method to print conductive paths over 3D-printed cases was investigated, in which an actuator was embedded into a 3D-printed part. Popa et al. [14] explored the design of a 3D-printed autonomous mechatronic device, which consists of a battery powering a DC motor without wires. Although the idea of integrating 3D printing and embedding external building blocks containing electronic or mechanical devices has been explored before, the automation of the process and the design of robots that allow this integration still needs to be developed.

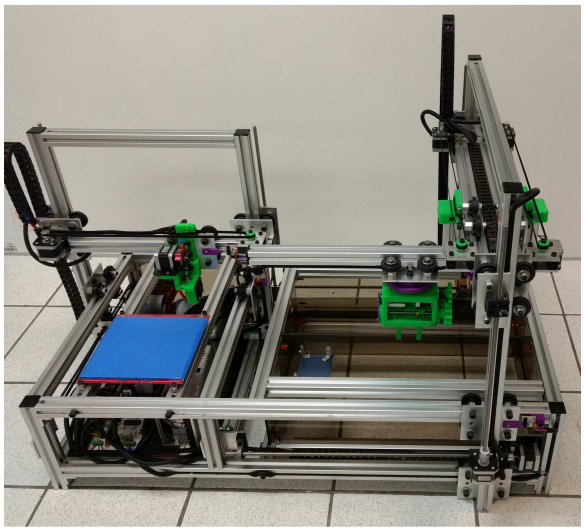

Fig. 1. Robot with 3D printing and pick and place modules integrated.

This paper introduces the design of a robot based on the FDM technology [1]. The robot comprises the 3D-printing and pick-and-place modules (Fig. 1). While the 3D-printing module fabricates the case of a device, the pick-and-place module selects a building block and places it into the case. The robot's functionality is validated by fabricating a device that is impossible to fabricate via classical 3D printing methods. The contributions of this work are summarised as follows: (i) The design of a robot that integrates 3D printing and automated assembly, and (ii) a methodology that defines the assembly process by integrating 3D printing.

The rest of this article is structured as follows. Section II summarises related works in 3D printing and assembly. Then, Section III details the design of the robot, followed by Section IV, which discusses the validation of the robot. Section V summarises the main challenges and highlights of this work. Finally, this paper is concluded in Section VI.

[1]Francisco Munguia-Galeano and Ze Ji are with the School of Engineering, Cardiff University, United Kingdom {MunguiaGaleanoF, ji2}@cardiff.ac.uk

[2]Lesli Ortega-Arroyo is with the School of Engineering, Anahuac University, Mexico leslie.ortegaar@anahuac.mx

[3]Miguel Gabriel Villarreal-Cervantes is with the Department of Mechatronics, CIDETEC, Instituto Politécnico Nacional, Mexico mvillarrealc@ipn.mx

[1]Demo available at https://youtu.be/Epk8p3CHJ4w

## II. Related work

Several studies have been conducted towards integrating building blocks into AM. For example, HotFlex [15] is a method in which a heated device is manually placed into a 3D-printed structure to mould and deform the part after it is printed. Another approach using building blocks is faBrickation [16], where pre-fabricated building blocks reduce printing times. In both approaches, the extra material is placed manually. On the other hand, the robot presented in this paper integrates a pick-and-place module that automatically embeds building blocks.

In the literature, there are approaches where extra material comes within the printer's extruder. In this context, Ambrosi et al. [17] proposed using electrochemical driving forces over different conductive materials, a method with the potential to reduce the complexity involved in the fabrication of electronic circuitry in general. Moukachar et al. [18] presented the design of a low-cost 3D printer that integrates various types of bio-inks, another example of using several materials in the extruder of the printer. However, the parts fabricated based on these approaches are still not complex enough to be considered a final product.

Regarding manufacturing final products based on AM, previous research has focused on 3D-printed electronics, which consist of embedding electronic components in a 3D-printed structure. For example, MacDonald et al. [19] presented the design of a six-sided gaming die that integrates a microprocessor and accelerometer. The authors proved that combining 3D printing and automatic assembly could drastically reduce new product development times. A more universal approach is presented in [20], where micromachining, laser welding, and conductive inks are complemented with FDM technology to fabricate complex electronic devices such as miniature satellites.

Another method to embed electronic components is the one presented by Kayfi et al. [21], in which copper wire and capacitive sensors are encapsulated within a 3D printed structure; this combination allows practical applications such as material and biomedical sensing. The manufacture of soft robots is another relevant application. Wehner et al. [22] introduced a method to print the body and microfluidic logic of a robot employing the SLA technology, pneumatic actuator networks are controlled using fuel reservoirs and catalytic reaction chambers, and at the end, a fully functional octopus-shaped robot is fabricated.

The approaches mentioned above of embedding electronic components and multi-materials in a 3D-printed structure are challenging and hold potential applications in many fields. Despite the advances in technologies and applications, the automation of embedding different types of materials and components still needs to be solved. Therefore, the novelty of the robot presented in this paper is in integrating AM and automated assembly, aiming to incorporate embedded building blocks to increase the functionality of 3D-printed parts and reduce the dependence on external production processes to fabricate a final product.

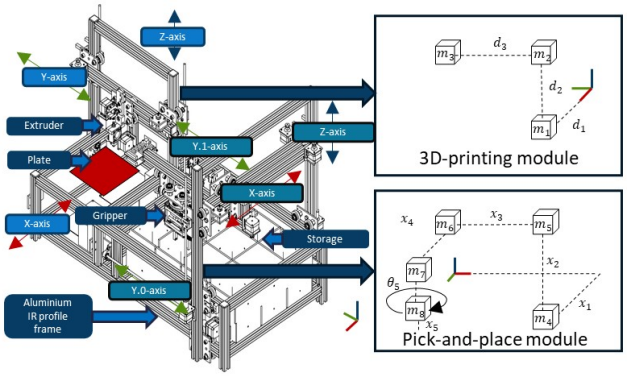


Fig. 2. This figure shows the main components of the robot, including the masses of the 3D printing and pick-and-place modules, as well as the extruder, plate, gripper, and storage. The figure also indicates the axes along which each joint moves.

## III. Design

The design method consists of dividing the system into the printing and pick-and-place modules. The printing module is in charge of fabricating the case of the object by depositing material from the printing nozzle, while the robot can place pre-assembled building blocks into the object using the pick-and-place module. The following are the system specifications:

1) Printing material: polylactic acid (PLA) and acrylonitrile butadiene styrene (ABS)
2) Print size of 20 $\times$ 20 $\times$ 20 cm.
3) Layer thickness of 0.2 mm.
4) The printer's maximum velocity and acceleration are 5 cm/s and 0.3 m/s$^2$, respectively.
5) The resolution of the X and Y axes is 0.025 mm.
6) The pick-and-place module's maximum velocity and acceleration are 2 cm/s and 0.1 m/s$^2$, respectively.
7) Extruder's temperature range: 100 °C to 250 °C.
8) Plates' (printing surface) temperature range: 40 °C to 100 °C.

### A. Mechanics

The frame of the robot (Fig. 2) is made from 30 $\times$ 30 mm aluminium IR profile, which is commonly used for automation applications. These profiles are made of an alloy of 6061-T6 aluminium with magnesium and silicon. Another essential characteristic is its shape, which allows for the building of structures in a simple way. Besides, the slits are suitable for use as linear rails, which are ideal for manufacturing prismatic joints.

The forward kinematics of the robot were calculated using the Denavit-Hartenberg (DH) convention. To actuate the joints of the 3D printer module, it is necessary to choose actuators that can exert sufficient force or torque to move them at the specified acceleration and velocity. Furthermore, to simplify the selection of the motors, the friction was eliminated due to the presence of bearings with a low coefficient of friction. The linear force is expressed as follows:

$$F_i = \frac{d}{dt}\frac{\partial L}{\partial \dot{d}_i} - \frac{\partial L}{\partial d_i}, \tag{1}$$

where $L$ is the Lagrangian of the system. Whereas for revolute joints, the torque is given by:

$$\tau_i = \frac{d}{dt}\frac{\partial L}{\partial \dot{\theta}_i} - \frac{\partial L}{\partial \theta_i} \tag{2}$$

The Lagrangian function is given by the following:

$$L = K - P, \tag{3}$$

where $K$ and $P$ are the kinetic and potential energies of the system, respectively. For the printer module, its kinetic energy is given by:

$$K_{3D} = \frac{1}{2}[(m_1+m_2+m_3)\dot{d}_1^2 + (m_2+m_3)\dot{d}_2^2 + m_3\dot{d}_3^2], \tag{4}$$

where $m_i$ and $\dot{d}_i \ \forall \ i = 1, ..., 3$ are the masses and joint's linear velocities of the $i-th$ link, respectively. The potential energy of the 3D-printing module is given by:

$$P_{3D} = d_2 g(m_2 + m_3) \tag{5}$$

where $d_2$ is the z-axis' height of the printer and $g$ is the acceleration of gravity equals 9.81 m/s$^2$. The kinetic energy of the pick-and-place module is given by:

$$\begin{aligned} K_{p\&p} = \frac{1}{2}[(m_4+m_5+m_6+m_7+m_8)\dot{x}_1^2 + \\ (m_5+m_6+m_7+m_8)\dot{x}_2^2 + (m_6+m_7+m_8)\dot{x}_3^2 + \\ (m_7+m_8)\dot{x}_4^2 + (m_7+m_8)\dot{x}_4\dot{x}_1 + I\dot{\theta}_5^2], \end{aligned} \tag{6}$$

where, the $m$ values are the masses of the links, $\dot{x}$ values are the joints' linear velocities, $\dot{\theta}_5^2$ is the angular velocity of the gripper and $I$ is its inertia matrix. The potential energy of the pick-and-place module is given by:

$$P_{p\&p} = x_2 g(m_5+m_6+m_7+m_8) - x_5 m_5 g, \tag{7}$$

where $x_3$ and $x_5$ are the distances parallel to the z-axis of the pick-and-place module's third and fifth degrees of freedom,

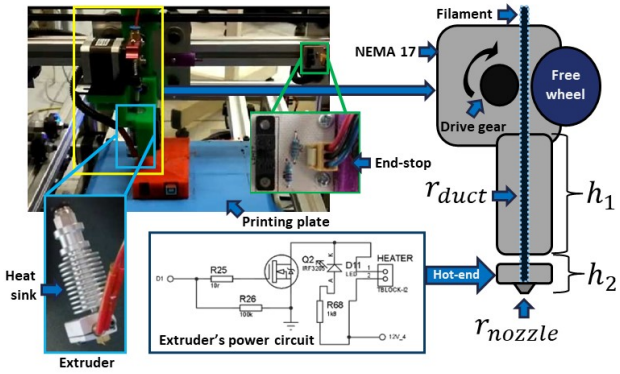


Fig. 3. This figure shows the extruder's mechanism to drive the filament, power circuit and main components (heat-sink, hot-end and nozzle). Besides, it displays an end-stop sensor.

which are affected by the gravity $g$. After applying equations (1) and (2) to the Lagrangian functions (equation (3)) of the 3D-printing and pick-and-place modules, it is possible to obtain the required forces and torques (Table I) for the robot to operate at the velocities and accelerations defined previously.

The joints actuated with a timing belt pulley mechanism use a GT2 pulley of 20 teeth and 12.5 mm in diameter. It is also known that NEMA 17 stepper motors can reach 0.57 Nm of torque. With this information and the torque equation:

$$\tau = F \times r, \tag{8}$$

where $r$ is the pulley's radio, it can be deduced that for the highest force required of $F_1 = 0.57$ N (Table I), the required torque while using the GT2 pulley is 3.7 $\times$ $1^{-3}$ Nm. This means that it is safe to use the NEMA 17 motors actuators of the robot that use timing belts.

In order to verify the suitability of the NEMA 17 motors for the joints actuated by screw spindles, it is necessary to calculate the work's relation between the input and output given by:

$$w_{in} = E \times w_{out}, \tag{9}$$

TABLE I

MECHANICAL CHARACTERISTICS OF THE ROBOT'S MODULES

| **3D printer module** | | | | | | | |
|---|---|---|---|---|---|---|---|
| **DOF** | **Axis** | **Mass (kg)** | **Joint type** | **Mechanism type** | **Force (N)** | **Torque (Nm)** | **Number of motors** |
| 1 | X | $m_1 = 0.25$ | Linear | Timing belt | $F_1 = 0.075$ | - | 1 |
| 2 | Z | $m_2 = 0.44$ | Linear | Timing belt | $F_2 = 0.57$ | - | 2 |
| 3 | Y | $m_3 = 1.2$ | Linear | Screw spindle | $F_3 = 11$ | - | 2 |
| **Pick-and-place module** | | | | | | | |
| **DOF** | **Axis actuation** | **Mass (kg)** | **Joint type** | **Mechanism type** | **Force (N)** | **Torque (Nm)** | **Number of motors** |
| 1 | Y | $m_4 = 1.8$ | Linear | Screw spindle | $F_1 = 0.14$ | - | 2 |
| 2 | Z | $m_5 = 1.25$ | Linear | Timing belt | $F_2 = 0.032$ | - | 1 |
| 3 | X | $m_6 = 2.31$ | Linear | Screw spindle | $F_3 = 40$ | - | 2 |
| 4 | Y | $m_7 = 0.8$ | Linear | Timing belt | $F_4 = 0.011$ | - | 1 |
| 5 | Z | $m_8 = 0.13$ | Revolute | Gear train | - | $\tau_5 = 2.15 \times 10^{-3}$ | 1 |

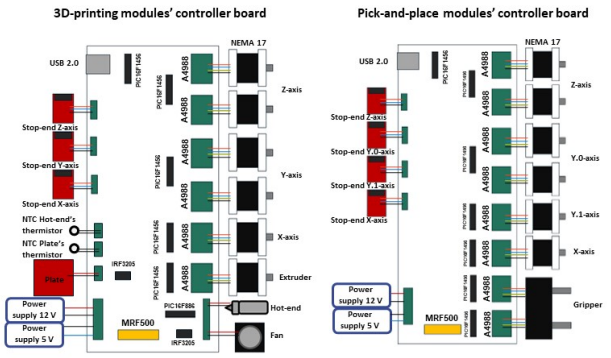


Fig. 4. This figure shows the robot's controller boards and circuit wiring.

where $w_{in}$ is the work of the motor, $w_{out}$ is the output's work in the nut of the screw, and $E$ is the efficiency of the screw given by:

$$E = \frac{1 - \mu \tan(\lambda)}{1 + \mu \cot(\lambda)}, \tag{10}$$

where $\mu$ is the friction coefficient between the screw spindle and nut (0.3 for friction between copper and steel) and $\lambda$ is the advance angle of the screw which can be deduced from the following:

$$tan(\lambda) = \frac{l}{\pi d_p}, \tag{11}$$

where $l$ is the diameter and $d_p$ the primitive diameter of the screw spindle. Since the screw spindles used in the robot have $l = 8$ mm and $d_p = 6$ mm, it can be calculated that the linear force a NEMA 17 can exert through a screw spindle with those characteristics is around 80 N, which is higher than the 40 N required by the third degree of freedom of the pick-and-place module (Table I). Hence, it is safe to use NEMA 17 motors for the screw spindle actuated joints of the robot.

Fig. 3 shows the extruder used by the 3D printer module, which comprises a heat sink at the top, a nozzle at the bottom, a heating resistance of 12 V and 40 W in and a 100K NTC (Negative Temperature Coefficient) thermistor. In order to prove the suitability of the NEMA 17 motor as a filament drive, the calculation of the linear force to make the filament flow is required. For this purpose, if the pressure exerted by the motor for driving the filament is greater than that of the melter, the filament flows through the extruder. To solve the problem, it is necessary to specify that the melted filament is an incompressible fluid, the velocity along the duct is constant, and the fluid has a constant viscosity. The following equation expresses the total pressure drop:

$$\Delta P = \Delta P_i + \Delta P_o, \tag{12}$$

where $\Delta P$ is the total pressure change in the extruder, $\Delta P_i$ is the pressure change at the nozzle inlet, and $\Delta P_o$ is the pressure change at the nozzle outlet. Newton's law of viscosity says that the shear stress in the fluid is given by:

$$\tau_{shear} = \mu \frac{dv}{dy}, \tag{13}$$

where $\tau_{shear}$ is the shear stress, $\mu$ is the dynamic viscosity and $\frac{dv}{dy}$ is the shear rate, given by:

$$\frac{dv}{dy} = \frac{4Q}{\pi r^3}, \tag{14}$$

where $r$ is the radius of the duct and $Q$ is the volumetric flow given by:

$$Q = v \times A, \tag{15}$$

where $A$ is the area of the duct, and $v$ is the velocity of the fluid. Besides Newton's law of viscosity, the shear stress can be expressed with the following:

$$\tau_{shear} = \frac{rP}{2h}, \tag{16}$$

where $h$ is the length of the duct. In order to solve for the pressure $P$ it is necessary to equalise equations (13) and (16), resulting in the following:

$$P = \frac{8h\mu v}{r^2} \tag{17}$$

With the equation (17), it is possible to calculate the pressures $\Delta P_i$ and $\Delta P_o$, corresponding to the inlet and outlet of the extruder, respectively. For the selected extruder (Fig. 3), the following data is given: $h_1 = 50$ mm, $h_2 = 5$ mm, $r_{duct} = 0.875$ mm, $r_{nozzle} = 0.2$ mm, $\mu = 10$ kPas, and $v = 50$ mm/s. The linear force required to make the filament flow is given by:

$$F = \Delta P \times \pi r_{drive}^2, \tag{18}$$

where the filament drive gear's radius $r_{drive}$ equals 5.25 mm. According to equation (12), the torque required to make the filament flow through the nozzle is around 0.34 Nm, lower than the 0.45 Nm that the NEMA 17 can exert. Hence, the motor is suitable for driving the filament through the extruder.

### *B. Electronics*

The controller boards (Fig. 4) are designed to communicate with a PC and control the NEMA 17 motors, as well as the temperature of the nozzle and printing plate. Each board controls either the 3D-printing or the pick-and-place module. The number of microcontrollers required is proportional to the number of NEMA 17 motors. Four power supplies are used, two providing 12 V for the stepper motors, heating and gripper and two providing 5 V for the microcontrollers. The electronic components of the controller boards were chosen based on the current and voltage consumption of the NEMA 17 motors, which require 1.7 A and 12 V, respectively. To achieve higher printing resolution, the controller boards integrate micro-stepping using A4988 drivers, widely used

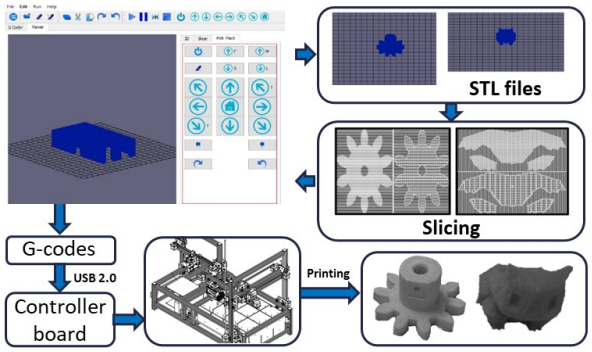


Fig. 5. The software utilises the STL files of the pieces to slice and transform them into g-codes that the controller board understands.

in open-source projects, that control the NEMA 17 motors. Additionally, MRF500 resettable fuses protect the controller boards.

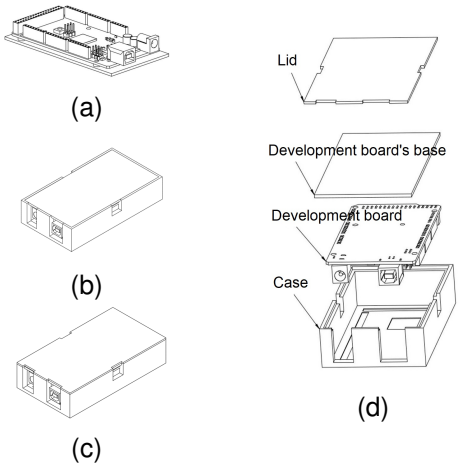


Fig. 6. Assembly process with 3D printing. (a) shows the pre-assembled building block. In (b), the building block is inserted into the object. (c) shows the device finished. (d) illustrates the objects' parts.

The controller boards use PIC16F1454 microcontrollers as they support communication via USB 2.0 and I2C. The datasheet of the A4988 driver indicates that it requires a current of 20 $\mu$A to operate, and the PIC16F1456 microcontroller can supply up to 25 mA on each pin, sufficient to operate the driver. The firmware of the controller boards was programmed in C language to understand g-codes and translate them into pulse signals for the drivers.

Since the extruder's hot-end and the heating device on the printing plate operates at 12 V and 40 W, the IRF3205 N-channel MOSFET, a fast-switching device, is used for temperature control. The voltage required to saturate the MOSFET's drain pin is $V_{DS(TH)} = 2$. Since using variable current is unnecessary, the MOSFET can be operated in saturation mode, which meets the condition $V_{DS} \geq V_{GS} - V_T$. According to the devices' datasheet, when 5 V are applied to the MOSFET's gate, the voltage between the drain and source, $V_{DS}$, reaches 1 V. Therefore, $V_{DS} \geq V_{GS}V_T$, indicating that the MOSFET is in saturation. To protect the microcontroller's control pin, the "R25" resistor (Fig. 3) is used to provide enough current to trigger the MOSFET. Additionally, to prevent unwanted states, the "R26" resistor (Fig. 3) is added in a pull-up configuration. The temperature of the hot-end and printing bed is measured using a 100K NTC thermistor. A PD controller is used to maintain a stable temperature for the nozzle and print plate. The PD control action is given by:

$$u = k_p e + k_d \dot{e}, \tag{19}$$

where $u$ is the control signal, $k_p$ is the proportional gain, $k_d$ is the derivative factor, $e$ is the error, and $\dot{e}$ is the derivative of error with respect to time. The device that controls the temperature is a PIC16F886. To this end, the controller board integrates end-stops sensors (Fig. 3) to set an initial motion reference for the 3D-printing and pick-and-place module.

### C. Software

The software (Fig. 5) used in this paper was developed in Python, aiming to allow the user to control the robot manually and automatically. To print parts, generating g-codes from the piece's STL file and the building block's position and orientation is necessary. Table II contains the list of instructions that the software and controller boards support.

TABLE II
G-CODES DESCRIPTION.

| Instruction | Description |
|---|---|
| ; | Comment |
| M06 | Changes tool |
| M82 | Sets absolute coordinates for the extruder |
| M104 X | Nozzle's temperature |
| M107 | Turn's fan on/off |
| M109 | Waits for the desired temperature to be reached |
| M190 X | Sets printing bed temperature |
| G1 | Straight line trayectory |
| G21 | Sets displacement units as mm |
| G28 | Home |
| G90 | Set absolute coordinates for the pick-and-place module |
| G92 | Reset extruder's distance |

The software utilises the following input parameters: the STL file of the piece to print, position and orientation of the building blocks to be inserted, nozzle size and temperature, printing bed temperature, printing velocity, and filling shape of the piece. The instructions that begin with M control the physical parameters of the robot (temperature, tool change, the extruder's and gripper's opening and rotation), while the codes starting with G control the displacement of both modules. To this end, the g-codes are sent through the USB port to the controller boards, which can interpret the instructions and translate them into pulses for controlling the NEMA 17 motors and the heating devices.

## IV. Validation

The object in Fig. 6c is used to validate the prototype empirically. The object comprises four parts, as displayed

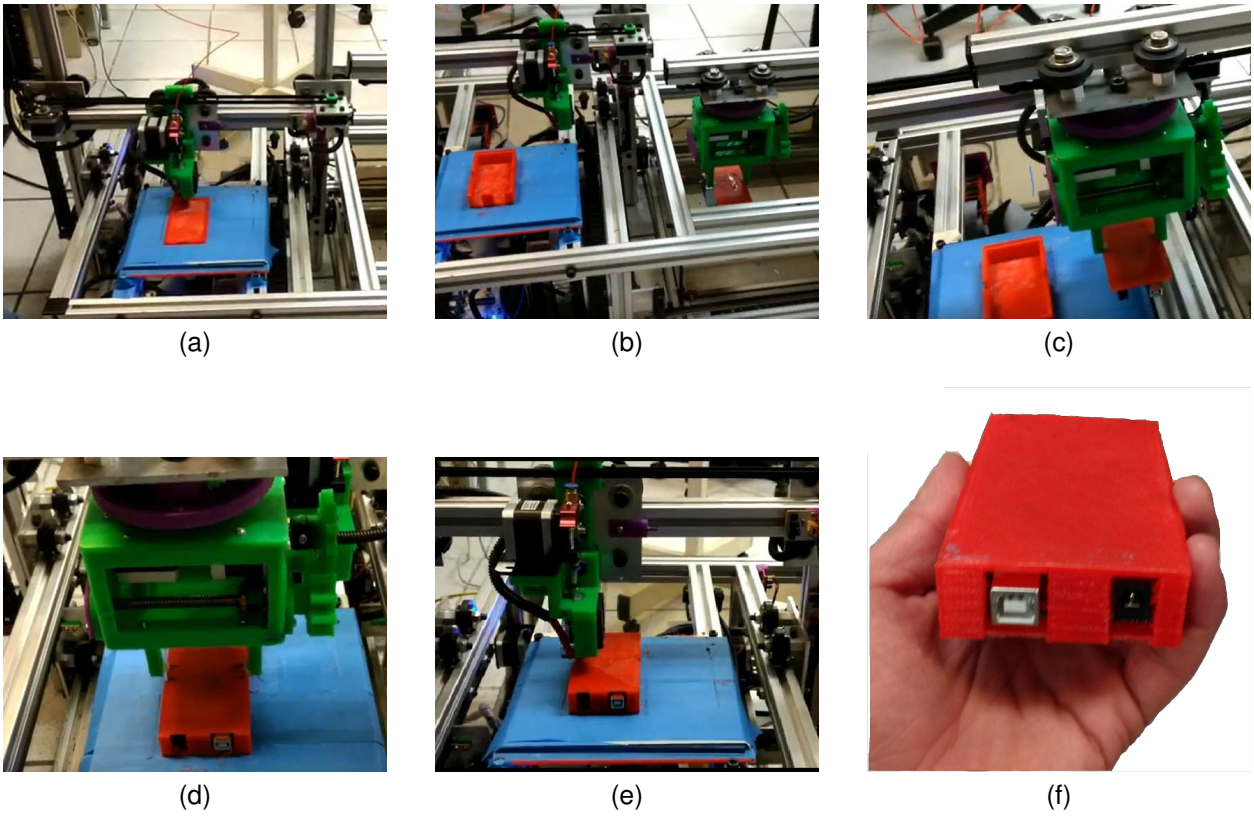


Fig. 7. In (a), the 3D-printing module prints part of the case. In (b), the pick-and-place module picks the building block. In (c), the pick-and-place module moves the gripper towards the case's location. In (d), the pick-and-place module places the building block into the case. In (e), the 3D-printing module prints the lid. (f) shows the finished product.

in Fig. 6c: case, development board, development board's base, and lid. Even though the 3D-printing module can print the case and lid, it cannot fabricate the building block that conforms to the development board and its base. The following steps are expected to be performed by the robot:

- The 3D-printing module fabricates the bottom part of the case.
- The pick-and-place module fits the building block into the case (Fig. 6b).
- The process ends when the 3D-printing module seals tha case by printing the lid.

The process described above was performed on the real robot (Fig. 7), which took around 4 hours to complete. First, the 3D-printing module fabricated the bottom part of the case as shown in Fig. 7a. Then, the pick-and-place module grabs the building block (Fig. 7b) and places it into the case (Fig. 7c). Once the object was fitted (Fig. 7d), the 3D-printing module sealed it by fabricating the lid. The finished product is shown in Fig. 7e. A demo of the robot manufacturing the device is available at `https://youtu.be/Epk8p3CHJ4w`

## V. Discussion

The proposed design offers several advantages, including expanding the current building capabilities of 3D printers. This paper demonstrated that the proposed robot could fabricate parts beyond traditional 3D printing methods by performing assembly tasks through the manipulation of distinct objects. The chosen structure of the robot, instead of an industrial robotic arm, offers the advantage of being an affordable choice due to its low cost. While industrial robotic arms can provide robustness and precise movements, they tend to be more expensive and often beyond the economic reach of researchers in developed countries. The robot designed in this paper allows for low-cost manufacturing while maintaining functionality. In terms of design challenges, the main difficulty was to identify suitable components that could meet the low-cost budget while still ensuring a robust and visually appealing design.

Moreover, the functionality of a 3D printer with assembly capabilities opens up new possibilities. The robot introduced in this paper has the potential to build a wide range of objects, such as mechanisms, gearboxes with integrated motors, robotic components, embedded sensors, and prototypes for user interface design. By prioritising cost considerations and exploring more affordable options, it may be possible to make this technology accessible to a wider range of users and applications.

## VI. Conclusions

This paper presented the design and validation of a robot that integrates 3D printing and automated assembly. The po-

tential applications of this robot were demonstrated through the fabrication of one object that can not be fabricated with traditional 3D printers due to the drawback of lacking a more diverse set of materials. The major limitation of this system lies in the positions where the pick-and-place module can put the pre-assembled building blocks and where the 3D-printing module can deposit material. Therefore, future work will focus on increasing the degrees of freedom of both modules to allow 3D printing in different positions and the insertion of a broader range of components. Additionally, the fabrication of more complex devices, such as gearboxes, embedded sensors and robotic devices, will be explored.

## ACKNOWLEDGEMENT

This work was partially supported by Consejo Nacional de Humanidades, Ciencias y Tecnologías.

## REFERENCES

[1] Q. Ji, X. Zhang, M. Chen, X. V. Wang, L. Wang and L. Feng, "Design and closed loop control of a 3D printed soft actuator," 2020 IEEE 16th International Conference on Automation Science and Engineering (CASE), Hong Kong, China, 2020, pp. 842-848, doi: 10.1109/CASE48305.2020.9216946.

[2] H. Kodama, "Automatic method for fabricating a three-dimensional plastic model with photo-hardening polymer", Review of Scientific Instruments, vol. 52, no. 11, pp. 1770-1773, 1981.

[3] K. Cooper, Rapid Prototyping Technology, Marcel Dekker, 2001.

[4] F. Parisi, A. M. Mangini, M. P. Fanti and N. Parisi, "A Drone-Assisted 3D Printing by Crane Structures in Construction Industry," 2021 IEEE 17th International Conference on Automation Science and Engineering (CASE), Lyon, France, 2021, pp. 171-176, doi: 10.1109/CASE49439.2021.9551611.

[5] Wong, Kaufui V., and Aldo Hernandez. "A review of additive manufacturing." International scholarly research notices 2012 (2012).

[6] Mohamed, Omar A., Syed H. Masood, and Jahar L. Bhowmik. "Optimization of fused deposition modeling process parameters: a review of current research and future prospects." Advances in manufacturing 3, no. 1 (2015): 42-53.

[7] J. Maas, B. Liu, S. Hajela, Y. Huang, X. Gong and W. J. Chappell, "Laser-Based Layer-by-Layer Polymer Stereolithography for High-Frequency Applications," in Proceedings of the IEEE, vol. 105, no. 4, pp. 645-654, April 2017, doi: 10.1109/JPROC.2016.2629179.

[8] E. H. Childs, A. V. Latchman, A. C. Lamont, J. D. Hubbard and R. D. Sochol, "Additive Assembly for PolyJet-Based Multi-Material 3D Printed Microfluidics," in Journal of Microelectromechanical Systems, vol. 29, no. 5, pp. 1094-1096, Oct. 2020, doi: 10.1109/JMEMS.2020.3003858.

[9] B. G. Mekonnen, G. Bright, and A. Walker, "A study on state of the art technology of laminated object manufacturing (LOM)," in Proc. 28th Int. Conf. on CAD/CAM, Robotics and Factories of the Future (CARs & FoF), 2016, pp. 207-216, Springer India.

[10] J.-P. Kruth, X. Wang, T. Laoui, and L. Froyen, "Lasers and materials in selective laser sintering," Assembly Automation, vol. 23, no. 4, pp. 357-371, 2003.

[11] L. E. Murr et al., "Metal fabrication by additive manufacturing using laser and electron beam melting technologies," Journal of Materials Science & Technology, vol. 28, no. 1, pp. 1-14, 2012.

[12] C. Kim et al., "3D Printed Electronics With High Performance, Multi-Layered Electrical Interconnect," in IEEE Access, vol. 5, pp. 25286-25294, 2017, doi: 10.1109/ACCESS.2017.2773571.

[13] A. -A. Popa, C. Mai, L. Duggen and J. Jouffroy, "Towards Printing Mechatronics: Considerations for 3D-printed conductive coupling," 2018 IEEE/ASME International Conference on Advanced Intelligent Mechatronics (AIM), Auckland, New Zealand, 2018, pp. 827-832, doi: 10.1109/AIM.2018.8452439.

[14] A. -A. Popa, L. Duggen and J. Jouffroy, "Towards Printing Mechatronics: An optimized battery-powered 3D-printed coupling design," 2019 IEEE/ASME International Conference on Advanced Intelligent Mechatronics (AIM), Hong Kong, China, 2019, pp. 418-423, doi: 10.1109/AIM.2019.8868575.

[15] K. F. Li, M. K. Y. Leung, and K. W. K. Wong, "HotFlex: Post-print Customization of 3D Prints Using Embedded State Change," in IEEE Transactions on Visualization and Computer Graphics, vol. 24, no. 5, pp. 1782-1792, May 2018, doi: 10.1109/TVCG.2018.2794628.

[16] S. Mueller, T. Mohr, K. Guenther, J. Frohnhofen, and P. Baudisch, "faBrickation: fast 3D printing of functional objects by integrating construction kit building blocks," in Proceedings of the SIGCHI Conference on Human Factors in Computing Systems, 2014, pp. 3827-3834, doi: 10.1145/2556288.2557032.

[17] A. Ambrosi, R. D. Webster, and M. Pumera, "Electrochemically driven multi-material 3D-printing," Applied Materials Today, vol. 18, p. 100530, 2020, doi: 10.1016/j.apmt.2019.100530.

[18] A. Moukachar et al., "Development and evaluation of a low-cost lego 3D bioprinter: from building-blocks to building blocks of life," Advanced Materials Technologies, vol. 8, p. 2100868, 2023, doi: 10.1002/admt.202100868.

[19] E. Macdonald et al., "3D Printing for the Rapid Prototyping of Structural Electronics," in IEEE Access, vol. 2, pp. 234-242, Dec. 2014, doi: 10.1109/ACCESS.2014.2311810.

[20] D. Espalin, D. Muse, E. MacDonald, and R. Wicker, "3D Printing multifunctionality: structures with electronics," International Journal of Advanced Manufacturing Technology, vol. 72, pp. 963-978, 2014, doi: 10.1007/s00170-014-6025-5.

[21] R. Kayfi, D. Ragab and T. A. Tutunji, "Mechatronic system design project: A 3D printer case study," 2015 IEEE Jordan Conference on Applied Electrical Engineering and Computing Technologies (AEECT), Amman, Jordan, 2015, pp. 1-6, doi: 10.1109/AEECT.2015.7360570.

[22] M. Wehner, R. L. Truby, D. J. Fitzgerald, B. Mosadegh, G. M. Whitesides, J. A. Lewis and R. J. Wood, "An integrated design and fabrication strategy for entirely soft, autonomous robots," Nature, vol. 536, no. 7617, pp. 451-455, Aug. 2016.